

Nonlinear aerostatic stability analysis of Hutong cable-stayed rail-cum-road bridge

Man Xu^{*}, Weiwei Guo^a, He Xia^b and Kebing Li

School of Civil Engineering, Beijing Jiaotong University, Beijing 100044, China

(Received March 21, 2016, Revised September 9, 2016, Accepted September 12, 2016)

Abstract. To investigate the nonlinear aerostatic stability of the Hutong cable-stayed rail-cum-road bridge with ultra-kilometer main span, a FEM bridge model is established. The tri-component wind loads and geometric nonlinearity are taken into consideration and discussed for the influence of nonlinear parameters and factors on bridge resistant capacity of aerostatic instability. The results show that the effect of initial wind attack-angle is significant for the aerostatic stability analysis of the bridge. The geometric nonlinearities of the bridge are of considerable importance in the analysis, especially the effect of cable sag. The instable mechanism of the Hutong Bridge with a steel truss girder is the spatial combination of vertical bending and torsion with large lateral bending displacement. The design wind velocity is much lower than the static instability wind velocity, and the structural aerostatic resistance capacity can meet the requirement.

Keywords: cable-stayed bridge; long span; aerostatic stability; geometric nonlinearity; wind attack-angle; tri-component wind loads

1. Introduction

The development of engineering theories and constructions raises the possibility of long span bridges over rivers and straits all over the world. Cable-stayed bridges have made rapid developments and the span length has exceeded 1000 m. In nowadays, cable-stayed bridges take a great part of long span bridges. For example, the Normandy bridge in France with main span 856 m, the Tatara bridge in Japan with main span 890 m, the Stonecutters bridge in Hong Kong with main span 1018 m, the Sutong Bridge in China with main span 1088 m and so on. Several researches about long span bridges have been done to study their characteristics (Huang, Seresh *et al.* 2013). The wind force scale over rivers and straits is usually quite large, which may influence bridges significantly. Due to the increase of main span, the long span bridges tend to be more flexible and sensitive to aerostatic instability (Fu, Wang *et al.* 2015). Besides, experimental observations suggest that long-span bridges are vulnerable to aerostatic instability. Therefore, aerostatic instability analysis is of considerable importance for long span bridges. Based on the aerostatic parameters from wind tunnel test, Li, Wang *et al.* (2014a) studied the aerostatic response

^{*}Corresponding author, Ph.D., E-mail: mendy1085@hotmail.com

^a Associate Professor, E-mail: junedragon@163.com

^b Professor, E-mail: hxia88@163.com

of the Hong Kong-Zhuhai-Macao Great Bridge in construction stage, found out the maximum deformation point of the bridge and checked the critical aerostatic instability wind velocity.

Aerostatic instability is a coupling effect of static wind loads and structural deformation (Zhang, Ge *et al.* 2013). When the deformed structure cannot resist the wind force and inversely enlarges the displacement-dependent tri-component wind loads, the aerostatic instability of the structure occurs (Cheng, Jiang *et al.* 2002). Boonyapinyo, Lauhatanon *et al.* (1994) discussed the wind induced nonlinear behavior of cable-stayed bridges, and according to the modes of static instability, categorized aerostatic instability into two types: torsional divergence and lateral-torsional buckling.

The Wind-resistant Design Specification for Highway Bridges (2004) suggests a linear method to analyze the critical aerostatic instability wind velocity of cable-stayed bridges, where the wind velocity is the function of bridge characteristics, including the height and width of the section, the mass and mass inertia moment of girder and cables, the fundamental frequencies of torsion and bending modes, and the tri-component wind load coefficients. However, the results from the linear method tend to be quite optimistic and to overestimate the aerostatic resistant capacity of long span bridges. Some researches introduced nonlinear FEM to the aerostatic instability analysis. Boonyapinyo, Lauhatanon *et al.* (2006) applied a nonlinear method that combines eigenvalue analysis and updated bound algorithms, to investigate the wind-induced nonlinear lateral-torsional buckling of cable-stayed bridges. Cheng, Jiang *et al.* (2003) proposed a nonlinear method based on the incremental two-iterative solution scheme for aerostatic stability problems of long span bridges, which has been widely used nowadays (Zhang, Ge *et al.* 2013a, b, Li, Wang *et al.* 2014a, b).

Researchers have studied the wind-induced aerostatic buckling for long span bridges. Zhang, Ge *et al.* (2013a) analyzed the aerostatic instability of a multiple-span suspension bridge over the Yangtze River, considering the spatial non-uniformity of wind velocity. Zhang and Yao (2015) performed numerical investigation on the wind-induced deformation of super long-span cable-stayed bridges, and discussed their aerostatic stabilities. Xu, Chen *et al.* (2013) carried out the aerostatic analysis on the Sutong Bridge, a 1088 m span cable-stayed bridge, and discussed the influences of pile foundation, cable sections and participation in modes, different initial and additional attack-angle, different wind profile and flows on deck displacement, pylon displacement, different modal frequencies and critical wind velocities. Wang and Xiong (2011) studied the wind resistance strategy and stability of a single-span suspension bridge, checked the structure stability under wind loads, and discussed the effect of cable index on structural wind resistance. These researches showed that the incorporation of the tri-component displacement-dependent wind loads and the geometric nonlinearity in the analysis resulted in a significant reduction in the critical wind velocity for aerostatic instability. With the increase of span length, the bridge structure becomes more flexible, and aerostatic instability studies for long span bridges need to be carried out.

However, most of nowadays analyses of aerostatic instability focused on the bridges with steel box-girder. The analysis of bridges with steel truss girder, one of the most common forms for long span rail-cum-road bridges, has rarely been studied. The characteristics under wind forces, the aerostatic stability capacity, the instability mechanism of truss girder and the influence of nonlinearities were barely known and discussed. In this regard, this paper takes the Hutong cable-stayed bridge with the main span of 1092 m as the case study, to investigate its aerostatic stability based on nonlinear analysis. Besides, as the combination of box-truss girder is first used in long span bridges, the structural characteristics and aerostatic behavior are analyzed.

2. Theoretical background

The stability problem of a bridge under wind load is the combination of the nonlinear aerostatic load behavior and nonlinear bridge response (Zhang, Ge *et al.* 2013a). The nonlinear aerostatic load behavior is induced by the spatial distribution of wind velocity and the displacement-dependent tri-components wind load.

2.1 Wind load

The stochastic wind field of a long span bridge can be defined by three dimensional (longitudinal, cross and vertical) wind components. As the correlations among the three dimensional turbulent wind components are weak, in practical analysis, the correlated three-dimensional wind field can be theoretically simplified as three independent one-dimensional wind fields (Xia, Roeck *et al.* 2011). This paper analyzes the bridge aerostatic instability under the cross winds since they are the most unfavorable design loads. The wind field characteristics discussed below focus on the cross wind component only.

2.1.1 The spatial distribution of wind velocity

The wind velocity changes with the altitude, as shown in Fig. 1. When the wind velocity V_0 at altitude H_0 is known, the wind velocity V_z at a certain altitude H_z can be obtained with the ground roughness height which depends on the landform condition.

According to Xia, Roeck *et al.* (2011), the ground roughness height for the Hutong Bridge site is taken as 0.01 m. The wind velocity on various tower sections can be calculated by the known wind velocity on the girder, the height of the top point and the ground roughness height. For example, according to local hydro meteorology condition of the Hutong Bridge, the design wind velocity is 38 m/s on the girder and the calculated wind velocity on the top of the tower is 45.28 m/s. The wind velocities of other tower sections can be calculated by means of the spatial distribution curve.

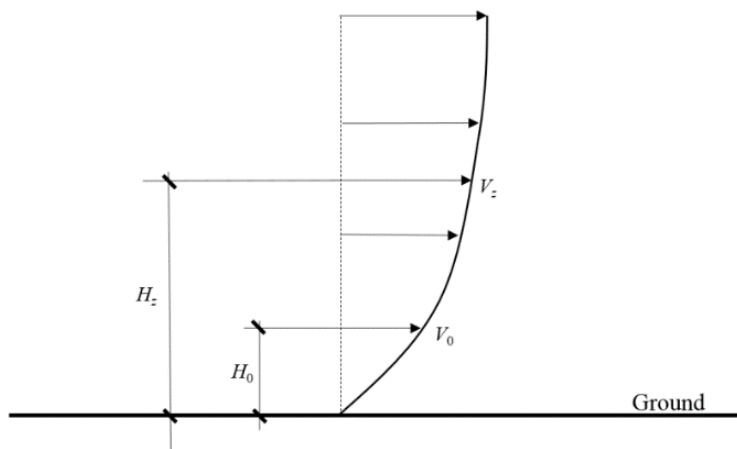


Fig. 1 The spatial distribution of wind velocity

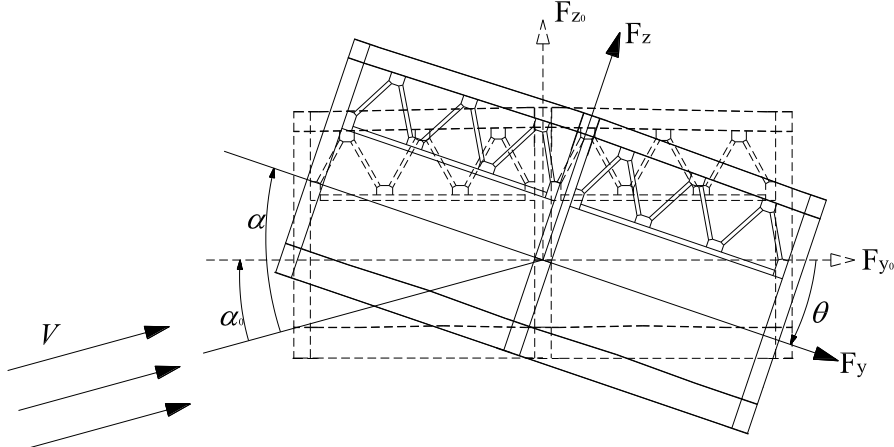


Fig. 2 Three components of wind load in different axes

2.1.2 The aerostatic wind force

The wind force consists of three components, drag force, lift force and pitch moment, as shown in Fig. 2. With the initial wind attack angle α_0 , the girder section twists to a torsion displacement θ , the local coordinates F_{y0} and F_{z0} turn to F_y and F_z , and the effective wind attack angle becomes α , which is the sum of initial wind attack angle α_0 and torsional displacement θ . The wind forces per unit span can be written as the function of effective wind attack angle in wind axes

$$\text{Drag force: } F_y = \frac{1}{2} \rho v^2 C_y(\alpha) D \quad (1a)$$

$$\text{Lift force: } F_z = \frac{1}{2} \rho v^2 C_z(\alpha) B \quad (1b)$$

$$\text{Pitch moment: } M = \frac{1}{2} \rho v^2 C_M(\alpha) B^2 \quad (1c)$$

where, $C_y(\alpha)$, $C_z(\alpha)$ and $C_M(\alpha)$ are the coefficients of drag force, lift force and pitch moment in the wind axes, respectively; α is the effective wind attack angle; ρ is the air density; B is the section width; D is the vertical projected area of the section.

2.2 Geometric nonlinearities of structure

The nonlinear incremental equilibrium equation under the tri-component wind loads can be written as

$$[K(u)] \cdot \{u\} = P(F_y(\alpha), F_z(\alpha), M(\alpha)) \quad (2)$$

$$K(u) = K_e(u) + K_g^{G+W}(u) \quad (3)$$

where, $K(u)$ is the structural stiffness matrix, which consists of two parts, the elastic stiffness matrix $K_e(u)$ and geometrical stiffness matrix $K_g^{G+W}(u)$, with the superscripts G and W representing gravity and wind loads, respectively; $\{u\}$ is the displacement vector.

A cable-stayed truss bridge mainly consists of three components: cables, towers and girders. The finite-element modeling of these components can be accomplished with two basic elements: link elements and beam elements. The geometric nonlinearities of a cable-stayed bridge originate from three primary sources: cable sag effect, combined axial load and bending moment interaction for the elements, and large displacement, which are produced by the geometry changes of the structure (Cheng, Jiang *et al.* 2002).

Normally, the sag effect of cables can be accounted with different methods by application of various elements: multi-link elements, catenary elements or single link element. In this paper, single link element is used and the equivalent modulus approach is applied for the sag effect. The Ernst equivalent modulus of elasticity is used. The modulus is related to the elastic modulus of cable material, the horizontal projected length of the cable, the cable weight per unit and the cable tensile stress.

The combined axial load and bending moment interaction normally appears in towers. In the study of bridge aerostatic instability, the girder is of the primary consideration. The influence of combined interaction on bridge aerostatic stability is slightly, so the combined interaction is not counted in this paper.

2.3 Solution procedure

The one-incremental and two-iterative solution scheme is used to solve Eq. (2) and to perform the analysis of the nonlinear aerostatic instability of cable-stayed bridge. In the method, the word “incremental” represents a certain increment of wind velocity. At each wind velocity increment, the internal cycle of iteration is performed to solve the nonlinear structural response by using the Newton-Raphson method. The structural response, such as the torsional deformation of the deck, would in turn affect the value of wind attack angle. And then the external cycle of iteration is performed to get the equilibrium of the additional wind forces and the structural response. When the scheme cannot obtain a convergent solution of the structural response under a certain wind velocity, the aerostatic instability occurs and the critical wind velocity can be found out. The procedures of this scheme can be summarized as follows:

- (1) Assume an original wind attack angle α_0 , and calculate the tri-component wind load coefficients $C_{y,z,M}(\alpha)$.
- (2) Assume an initial wind velocity V_0 and an increment ΔV , and let $V = V_0$.
- (3) Calculate the wind loads $F_{y,z,M}$ under the wind velocity V .
- (4) Solve Eq. (2), to calculate the structural displacement by the Newton-Raphson method.

With the deformation of bridge structure, the effective attack angle changes and the Euclidean norm of static tri-component wind force coefficients $C_{y,z,M}(\alpha)$ is calculated as

$$\text{Norm}_k = \left\{ \frac{\sum_{j=1}^{N_a} [C_k(\alpha_j) - C_k(\alpha_{j-1})]^2}{\sum_{j=1}^{N_a} [C_k(\alpha_j)]^2} \right\}^{1/2}, k = y, z, M \quad (4)$$

where, N_a is the number of nodes subjected to the displacement-depended wind load; j is the serial number of current iteration;

(6) Check whether or not the Euclidean norm of aerodynamic force coefficient is less than the prescribed tolerance ε_k , which is usually taken as 0.005, namely

$$\text{Norm}_k \leq \varepsilon_k, k = y, z, M \quad (5)$$

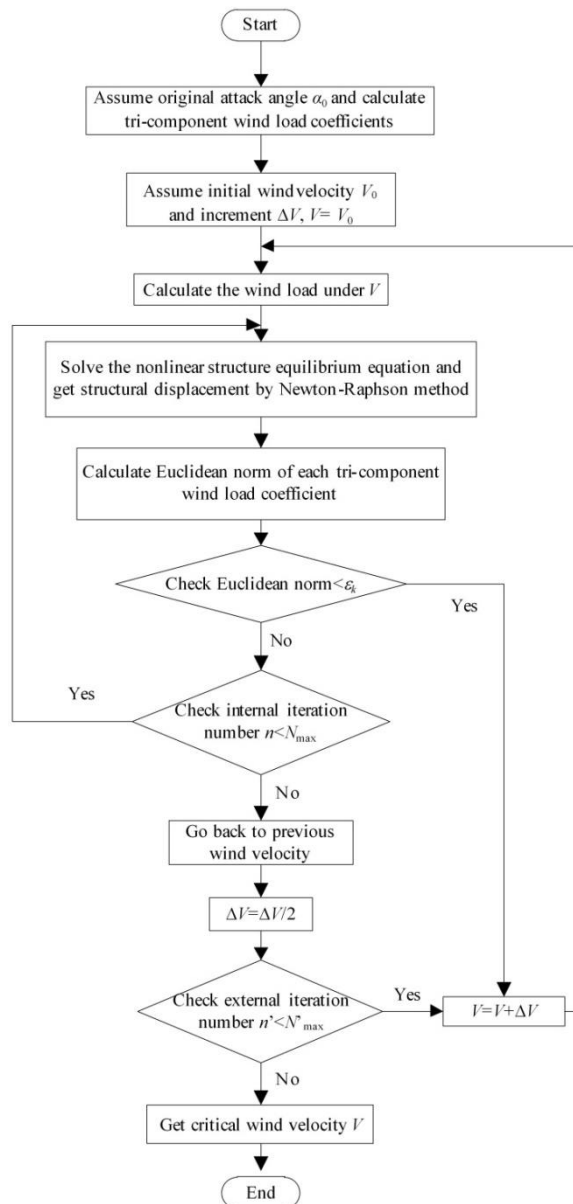


Fig. 3 Flow chart of the program for the solution procedures

(7) If Eq. (4) is satisfied, output the structural response result, and start the calculation for the next wind velocity $V = V + \Delta V$, by steps (3)-(6).

(8) If Eq.(4) is not satisfied, check whether or not the internal iteration number n is less than prescribed maximum number N_{\max} . If so, repeat steps (4)-(6).

(9) If the internal iteration number n is not less than N_{\max} , go back to the equilibrium state of previous wind velocity V , and shorten the wind velocity increment, letting $\Delta V = \Delta V/2$, to check whether or not the external iteration number n' is less than the prescribed maximum number N'_{\max} . If so, let $V = V + \Delta V$, and repeat steps (3)-(6).

(10) If the external iteration number n' is not less than N'_{\max} , the current wind velocity is taken as the critical wind velocity V .

Based on the steps, a program is developed and the flow chart is shown in Fig. 3.

3. Case study

3.1 Description of the Hutong Bridge

The Hutong Bridge over the Yangtze River is a cable-stayed rail-cum-road bridge with a 1092 m central span and two 462 m side spans. For the navigation requirement, two navigation spans with 142 m length are designed outside the two side spans. The bridge span arrangements are (142 + 462 + 1092 + 462 + 142) m. The heights of the two towers are both 271 m above the girder. The general configuration of the bridge is shown in Fig. 4. The girder section is shown in Fig. 5, and the panel length of the girder is 14 m. The 224 m long girders with concrete-steel compound highway deck is applied in the side spans, to increase the self-weight and to balance the negative reaction of the auxiliary piers.

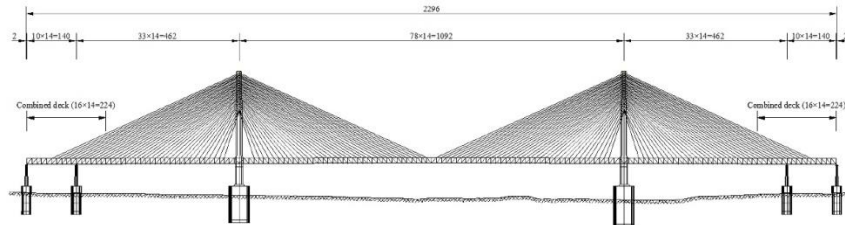


Fig. 4 Elevation of the Hutong Bridge (unit: m)

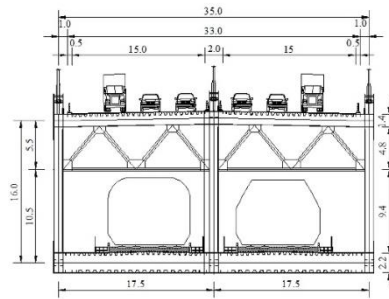


Fig. 5 Standard cross-sections of the bridge (unit: m)

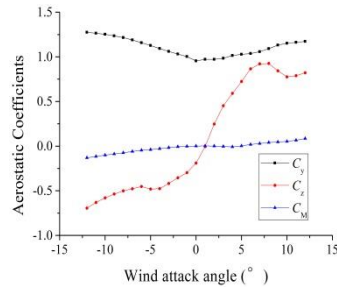


Fig. 6 Aerostatic coefficients of the girder model

Table 1 Drag load coefficients of the tower

Height range(m)	5.6-69.6	69.6-149.6	149.6-221.6	221.6-306.0
C_y	1.8	1.51	1.56	1.69

To investigate the tri-component wind load coefficients, a segment model test was carried out by the wind tunnel in the Southwest Jiaotong University (Zhang 2015), in which a reduced scale model with nine panels of the girder was made and tested. The curves of tri-component wind load coefficients varying with wind attack angles are obtained from the model test and shown in Fig. 6. As shown in the figure, as the wind attack angle ranges from 2° to 8° , the tri-component coefficients are positive and increase with the wind attack angle, which means the wind loads work together to tumble the bridge girder in this range.

As for the tower, only the drag load is taken into consideration. The drag wind load coefficients are referred from the Sutong Bridge (Xu and Chen 2009), as shown in Table 1.

Shown in Fig. 7 is the three-dimensional FE model for the Hutong bridge established by the commercial software ANSYS. The truss girder and towers are modeled by 3D beam elements, the cables by 3D link elements to account for the geometric nonlinearity due to cable sag, and the bridge deck by shell elements defined with the real material properties. The girder is simply supported to the two towers and four piers, where the lateral and vertical displacements of the girder are constrained. The 3D link elements for cables are defined with initial tensile prestress. The equivalent modulus of each cable element is calculated according to the cable characters, such as the material, the horizontal projected length, the weight per unit and the tensile stress of the cable, to consider the cable sag effect.

A modal analysis is carried out for the bridge model, to obtain the vibration characteristics including natural frequencies and mode shapes descriptions, as listed in Table 2. The first mode is lateral deflection with the natural frequency 0.083 Hz, which indicates that the stiffness in the lateral direction is small and the lateral deformation may occur more easily than others. Besides, as shown in Fig. 8, the deformation of the girder of the 1st mode is symmetric lateral bending with slightly torsion. For the main 1092 m span, the girder twists clockwise at the beam-ends and counterclockwise at the mid-span. The fundamental frequencies in the vertical direction and in torsion are 0.204 Hz and 0.581 Hz, respectively. The natural frequency of the torsion mode is

much larger than that of the lateral/vertical mode. The results of modal analysis show that the response of the bridge under external wind load can be supposed to be dominant lateral deflection.

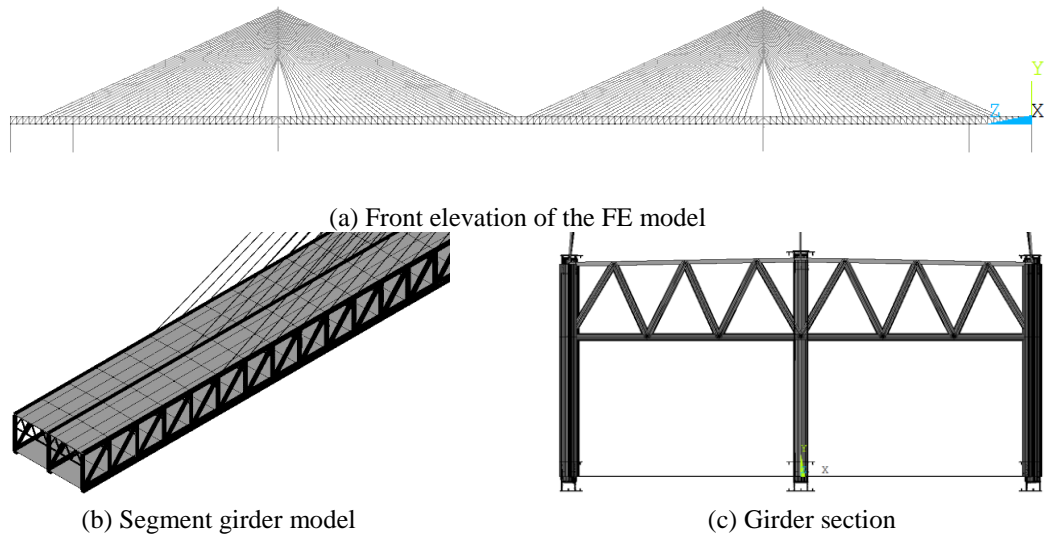
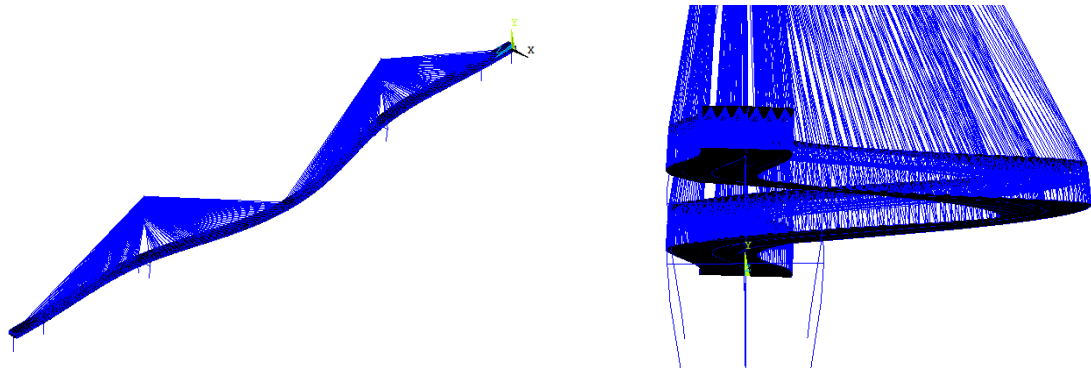


Fig. 7 The FE model of the Hutong Bridge

Table 2 Natural frequencies and mode descriptions of Hutong Bridge

No.	Frequency (Hz)	Mode description	No.	Frequency (Hz)	Mode description
1	0.083	1 st symmetrical lateral bending movement	9	0.431	3 rd symmetrical vertical bending movement
2	0.085	1 st floating movement	10	0.456	4 th anti-symmetrical bending- and-torsion movement
3	0.204	1 st vertical bending movement	11	0.504	4 th anti-symmetrical vertical bending movement
4	0.238	2 nd anti-symmetrical lateral bending movement	12	0.536	5 th symmetrical lateral bending- and-torsion movement
5	0.292	2 nd anti-symmetrical vertical bending movement	13	0.553	5 th symmetrical vertical bending movement
8	0.392	3 rd symmetrical lateral bending- and-weak torsion movement	14	0.581	1 st symmetrical torsion-and-weak lateral bending movement

Fig. 8 The mode shape of the 1st symmetric lateral bending mode

3.2 Effect of structural geometric nonlinearities

To explore the influence of the structural geometric nonlinearities including cable sag and large displacement on structural response, the results of bridge analysis under self-weight and secondary dead-load are discussed in this section.

Four cases are considered in the analysis: i) without geometric nonlinearity; ii) cable sag effect only; iii) large displacement effect only; iv) both cable sag and large displacement effects. The displacements at mid-span of the bridge under the four cases are listed in Table 3. In this analysis, the positive vertical displacement is upward.

Normally, the self-weight and secondary dead-loads are applied on the structure in the vertical direction. As a result, it is shown in Table 3 that the vertical displacement at mid-span is much obvious, and the values of lateral and torsional displacement are quite small. The structure responses are affected by the cable sag effect, resulting in the decrease of cable tensile forces and upwards deflection of the girder. Comparing Case i and Case ii, the vertical displacement decreases almost 16% when considering cable sag effect. However, the large displacement effect shows little influence on the structural responses.

Table 3 Displacements at mid-span of the bridge with different conditions

Case	Description	Lateral disp. (m)	Vertical disp. (m)	Torsional angle(°)
i	without nonlinearities	-0.140e-2	1.9248	0.337e-3
ii	cable sag only	-0.143e-2	1.6409	0.149e-3
iii	large disp. only	-0.140e-2	1.9248	0.337e-3
iv	ii +iii	-0.143e-2	1.6409	0.149e-3

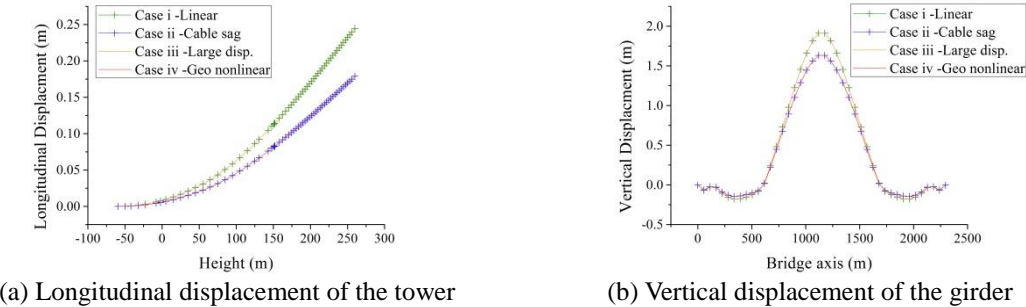


Fig. 9 Bridge displacement response in four cases

Similar results are shown in Fig. 9, where the bridge displacement responses under four cases are drawn. Fig. 9(a) shows the longitudinal displacement distribution of one of the towers. Along the tower height, the longitudinal displacement increases from almost zero to over 0.2 m. Fig. 9(b) gives the vertical displacement curves of the truss girder. The maximum value appears at the middle span. In both the two figures, it is shown that the cable sag effect plays a great role on the structure responses. The blue cross (Case ii: only cable sag effect) and red line curves (Case iv: both cable sag and large displacement effects) in Fig. 9 show different values from the other two. On the other hand, the influence of large displacement effect is too slightly to show up.

The comparison of the cases demonstrates that the geometric nonlinearity, especially the cable sag effect, has big effect on the bridge structural response under self-weight loads. In the bridge axial region 700 m to 1200 m and the tower over 150 m height, the effect of geometric nonlinearity is quite significant.

3.3 Aerostatic instability analysis

In this section, the aerostatic instability of the Hutong Bridge is analyzed by the proposed nonlinear program. Firstly, the whole-process aerostatic instability analysis with $\alpha_0 = 0$ is carried out to elaborate the critical stable wind velocity and the failure mechanism of the bridge under aerostatic loads. Then, the influence of different parameters on the critical wind velocity is studied and discussed.

3.3.1 System behavior of bridge under wind loads

According to the researches by Cheng *et al.* (2002, 2003, 2004), the loading path does not influence the final result, which means for a certain attack angle, the loading path will not change the structural response results. The following analysis are based on the wind loading path of initial wind velocity $V_0 = 50$ m/s and wind velocity increment $\Delta V = 10$ m/s.

According to the calculation procedures given in Fig. 3, when the wind velocity reaches 249 m/s, the structure shows unusual increments in displacements and the equilibrium position could not be found. Therefore, the velocity 249 m/s is taken as critical wind velocity in this case. Comparing to the design wind velocity 38 m/s of the Hutong Bridge, the critical wind velocity 249 m/s is over 5 times higher than the design wind, which can meet the requirement given in the specification (JTG/T D60-01--2004).

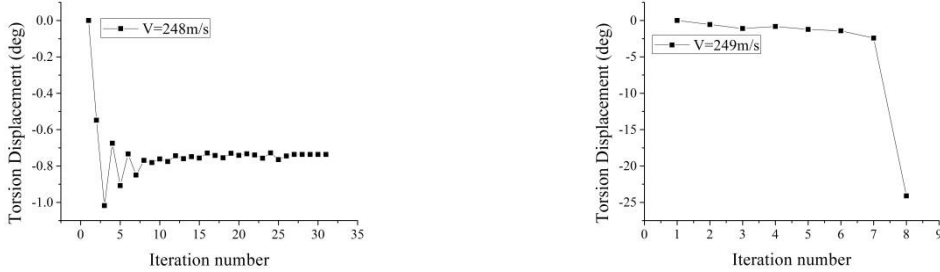


Fig. 10 Torsional displacement at mid-span vs iteration number

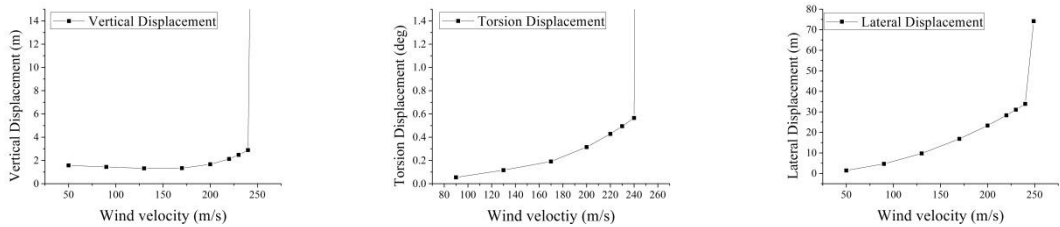


Fig. 11 Displacement behavior at the mid-span

Shown in Fig. 10 are the distributions of torsion displacement at the mid-span of the girder at wind velocities 248 m/s and 249 m/s vs iteration number, respectively. It can be seen that with the velocity (248 m/s) below the critical one, the mid-span torsional displacement can converge to a stable value after several times of iteration. While when the velocity reaches 249 m/s, the torsional displacement diverges after several iterations, indicating that the structure cannot get to an equilibrium position at the critical wind velocity.

The whole-progress displacement fluctuation at the mid-span is shown in Fig. 11. Before the wind velocity reaches the critical one (249 m/s), the displacements vary in a smaller region: the vertical displacement changes from 1.4 m to 2.8 m, the torsional angle gradually increases to 0.5 degree, the positive value of the torsional angle representing clockwise torsion, and the lateral displacement increases proportionally with wind velocity. Once the wind velocity reaches 249 m/s, the structure loses the critical resistance capacity of aerostatic stability and the displacements increase sharply to a large value.

Illustrated in Fig. 12 are the displacements of the girder at different wind velocities. It can be seen that the vertical and torsion displacements increase slightly with the wind velocity before the critical velocity (249 m/s), and in the situation of critical wind velocity, the values of them enlarge several times more than before. In the meantime, the lateral displacement increases gradually and reaches to a relatively large value at the critical wind velocity.

From Figs. 11 and 12 one can see how the critical wind velocity occurs. When the wind velocity is small, the displacement of the girder increases gradually with wind velocity. When the

wind velocity reaches a certain value, the so-called critical wind velocity, an unstable state appears, with the displacement increasing sharply to large amplitude, several times of the previous displacement. The sudden increment occurs in the vertical and torsional displacements, together with a large increment of lateral displacement. The instable process mechanism in this case is the instability in vertical bending and torsion, together with larger lateral bending displacement. Besides, according to the torsional displacement curves, the maximum value does not occur at the mid-span.

The lateral and longitudinal displacement of the tower under various wind velocities are shown in Fig. 13. It can be seen that both the lateral and longitudinal displacements increase along with the height of the tower. The lateral displacement curve of the tower increases gradually with the wind velocity, without significant increment at the critical wind velocity. The longitudinal displacement curve also increase gradually with the wind velocity, but at the critical wind velocity (249 m/s), it shows a sudden increase to a very large value.

Fig. 14 gives the cable stresses of the central/side span on both the windward and the leeward side. For the central span cables, with the increase of wind velocity, the cable stress on the windward side reduces gradually to a small value, while the stress on the leeward side increases a lot. Once the wind velocity reaches the critical value, the value of cable stress on the leeward side decreases suddenly to almost zero. Different behavior can be observed in the side span cables. Both the windward and leeward side cables stresses increase firstly with the wind velocity and then decrease gradually till the critical velocity, by then both the cable stresses reduce suddenly.

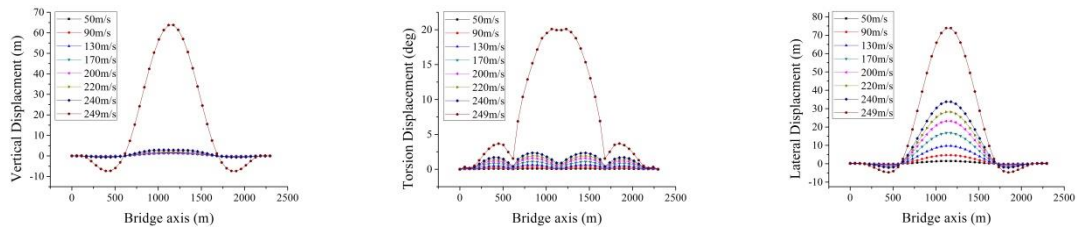


Fig. 12 Vertical, torsional, and lateral displacements of the girder at various wind velocities

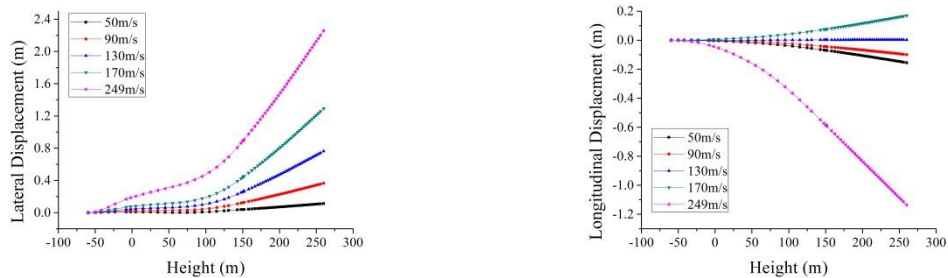


Fig. 13 Lateral and longitudinal displacement of the tower at various wind velocities

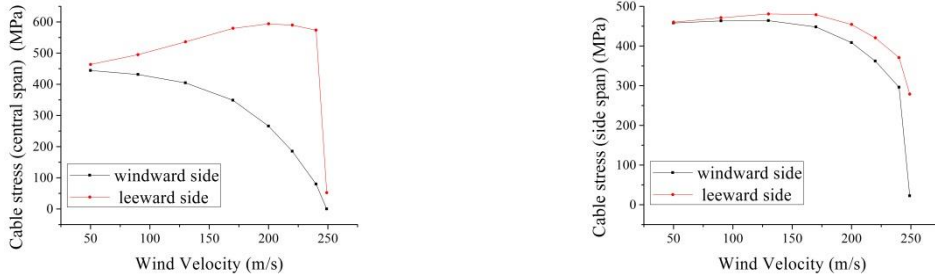


Fig. 14 Cable stress at various wind velocities

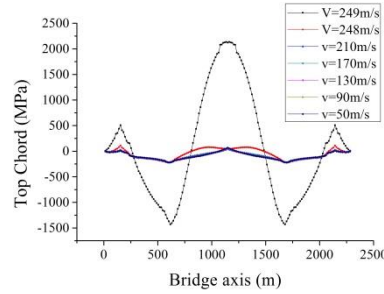


Fig. 15 Axial stress of the top chord at various wind velocities

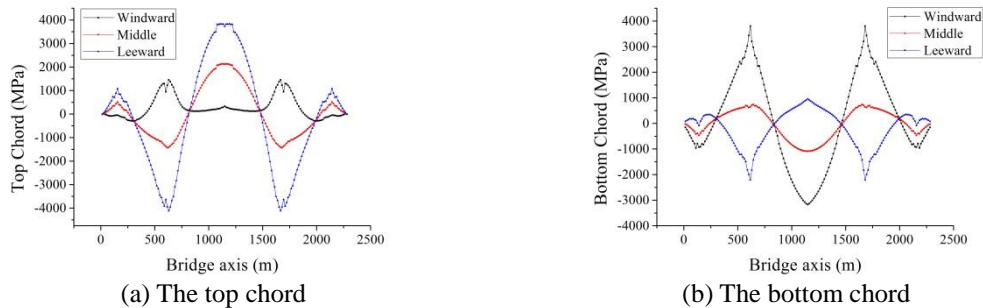


Fig. 16 Axial stress at critical wind velocity on the windward/middle/leeward side

The axial stresses of the truss members are of great importance in this case. Fig. 15 gives an example of the axial stress of the top chord at various wind velocities. Similar to the trend shown in Fig. 12, with the increase of wind velocity, the axial stress increases slightly until the wind velocity reaches the critical value, when the critical value of axial stress enlarges to over 10 times of the previous value. Fig. 16 compares the values of axial stresses of the chord members at different locations, on the windward, in the middle and on the leeward side. According to the curves, there are three critical locations where the axial stresses are quite large, the mid-span of the

main 1092 m span and the connection area near the towers. The maximum axial stress appears at the mid-span of the main span. With the critical wind velocity, referring to top chords, the axial stresses on the leeward side are much larger than the values on other locations. On the other hand, referring to the bottom chord, the critical values appear on the windward side.

The critical axial stress values and locations of different truss member types are given in Table 4. The positive value in the table represents tension stress. The critical value of chord axial stress appears at the middle span of the main 1092 m span. The critical axial stresses of vertical and slant rods are 1842.40 MPa (tension) and 2284.10 MPa (compression), respectively. The critical rod members are both near the 1/4-span of the main 1092 m span, on the windward side. The critical member is the bottom chord at the middle span of the main span on the windward side, with the maximum axial stress 4112.7 MPa (compression).

3.3.2 Effects of initial wind attack angles

The tri-components aerostatic wind loads are the function of wind attack-angle, thus the effect of initial wind attack-angle on the critical wind velocity needs to study. Different initial wind attack-angles are considered in the aerostatic instability analysis, and the results are shown in Table 5 and Fig. 17.

Table 4 Critical axial stresses and the locations

Truss member type	Critical value (MPa)	Location of Critical value
Top chord	3806.21	Mid-span of the main span on the leeward side
Bottom chord	-4112.7	Mid-span of the main span on the windward side
Vertical rod	1842.40	Near the 1/4-span of the main span on the windward side
Slant rod	-2284.10	Near the 1/4-span of the main span on the windward side

Table 5 Critical wind velocities at different wind attack-angles

Initial attack-angle α_0 (°)	Critical wind velocity V_{cr} (m/s)	Lateral displacement (m)	Vertical displacement (m)	Torsional angle (°)
-3	350	168.959	86.932	-32.448
-1	285	120.901	72.906	-27.585
0	249	74.154	64.048	-24.104
1	230	58.769	34.761	-15.417
3	197	31.005	10.549	-4.793
6	190	27.474	8.635	-3.547

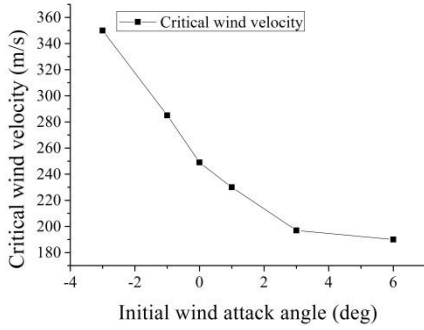


Fig. 17 Critical wind velocity of the bridge under different wind attack-angles

As shown in Table 5, on the one hand, the critical wind velocities of the structure with negative initial wind attack-angles are larger than the others, showing that the structure is more stable and not quite vulnerable to aerostatic instability. With the initial wind attack angles smaller than -3° , the critical wind velocities are supposed to be higher than 350 m/s, which are far more than the design value, so no details are proved here.

On the other hand, with positive initial wind attack-angles, the larger the initial attack-angles, the smaller the critical wind velocities. According to Sec. 3.1, as the wind attack-angle ranges from 2° to 8° , the tri-component wind forces increase with the attack-angle. Therefore, under the same wind velocity, the structure responses will increase with the initial wind attack-angle as well. With the increase of initial wind attack-angle, the structure becomes more instable, as shown in Table 5.

Besides, according to the table, in the initial wind attack-angle range $0^\circ \sim 3^\circ$, the critical wind velocities decrease a lot, from 249 m/s to 197 m/s, almost by 20% decrement. In the initial wind attack-angle range $3^\circ \sim 6^\circ$, the critical wind velocities decrease from 197 m/s to 190 m/s, only by 3.5%. This suggests that the structure aerostatic stability is more sensitive to angle change when the initial wind attack-angles are small. Therefore, it is reasonable to suppose that the critical wind velocities would not change much with the initial wind attack-angles more than 6° . The curve of critical wind velocity varies with initial critical wind attack-angle is shown in Fig. 17.

3.3.3 Effects of geometric nonlinearities

To investigate the effects of geometric nonlinearities on critical wind velocity, the geometric nonlinearities induced by cable sag, large displacement and their combination are considered. Table 6 shows the effects of the two types of geometric nonlinearities on the critical wind velocity and displacements at the mid-span of the bridge girder. The analysis is all carried out when $\alpha_0=0$.

As can be seen in the table, the geometric nonlinearities have influence on both the critical wind velocity and the structure displacements. Without considering the nonlinearities, the aerostatic instability of the bridge occurs at the critical wind velocity 266 m/s, with the lateral, vertical and torsional displacements 36.29 m, 85.35 m and -9.64° at the mid-span, respectively. When all the two geometric nonlinearities are considered, the nonlinear aerostatic instability occurs at a smaller critical wind velocity 249 m/s, with lateral, vertical and torsional displacements 74.15 m, 64.05 m and -24.10° , respectively.

Table 6 Effects of two types of geometric nonlinearities and aerostatic stability analysis results

Case	Nonlinear types	Critical wind velocity (m/s)	Lateral displacement (m)	Vertical displacement (m)	Torsional angle (°)
I	None (linear)	266	36.29	85.35	-9.64
II	Cable sag	260	42.35	42.05	-5.34
III	Large displacement	258	82.25	72.67	-31.12
IV	II+III	249	74.15	64.05	-24.10

When the geometric nonlinearity is considered (Cases II~IV), the critical wind velocities of the structure are smaller than that in the linear case. Besides, when the large displacement effect is considered (Cases III and IV), the displacements become much larger.

The comparison of the four cases shows that geometric nonlinearity has obvious influence on the aerostatic instability. With the geometric nonlinearity, the structure becomes vulnerable to aerostatic instability.

3.4 Aerostatic failure mechanism

The wind loads applied on the bridge structure consist of three components, the drag load, the lift load and the pitch moment. The drag load is always positive and increase with wind velocity, which enlarge the lateral structure displacement gradually. The directions of lift load and pitch moment change with wind attack-angle, leading to different trend of vertical and torsional displacement. The worst situation occurs when all the tri-component wind loads work together to tumble the girder.

Before the critical wind velocity, the structure deforms at an equilibrium state, with mainly lateral bending and slightly vertical bending and torsional deformation. For the main span of 1092 m, the girder twists clockwise at the beam-ends and anticlockwise at the mid-span. This behavior is a match with the mode shape of the 1st symmetric bending mode.

When the wind velocity reaches a certain value, the structure will lose its equilibrium state and the vertical and torsional displacements increase significantly to large values. In this case, the spatial bending-and-torsion aerostatic instability of the structure takes place, together with large lateral displacement.

4. Conclusions

This paper combines the wind load nonlinearity and geometric nonlinearities, applies the aerostatic instability analysis on the Hutong cable-stayed rail-cum-road bridge with a 1092 m main span. By means of the one-incremental and two-iterative solution scheme methods, the critical wind velocity of the bridge, the effects of different parameters and the aerostatic failure mechanism are analyzed. The conclusions are summarized as follows:

- The aerostatic failure pattern of the Hutong Bridge is the sudden increase of vertical and torsional displacement, which means the occurrence of combined spatial bending and torsional deformation, together with large lateral bending displacement.
- The initial wind attack-angle has a considerable effect on the aerostatic stability results. Negative initial wind attack-angles result in higher critical wind velocities. As for positive attack-angles, the critical wind velocity is more sensitive during small angle range ($0^\circ \sim 3^\circ$), and less sensitive in large initial wind attack-angles ($3^\circ \sim 6^\circ$).
- The aerostatic instability of the bridge is influenced by the geometric nonlinearity. Both the cable sag and large displacement effects play a role in structure aerostatic stability. The critical wind velocities in the cases when geometric nonlinearity is considered are smaller than that without nonlinearity. And the structural displacements under the influence of large displacement effect are larger than others.
- The design wind velocity (38 m/s) of the Hutong Bridge is much lower than the critical wind velocity (249 m/s). The structural aerostatic resistance capacity can meet the requirement of aerostatic stability.

Acknowledgements

The authors gratefully acknowledge the financial support provided by the National Basic Research Program (“973” Program, 2013CB036203) and the National Natural Science Foundations (51308034 and U1434205) of China.

References

- Boonyapinyo, V., Yamada, H. and Miyata T. (1994), “Wind-induced nonlinear lateral-torsional buckling of cable-stayed bridges”, *J. Struct. Div. - ASCE*, 486-506.
- Boonyapinyo, V., Lauhatanon, Y. and Lukkunaprasit P. (2006), “Nonlinear aerostatic stability analysis of suspension bridges”, *Eng. Struct.*, **28**(5), 793-803.
- Cheng, J., Jiang, J.J., Xiao, R.C. and Xiang, H.F. (2002), “Advanced aerostatic stability analysis of cable-stayed bridges using finite-element method”, *Comput. Struct.*, **80**, 1145-4458.
- Cheng, J., Jiang, J.J. and Xiao, R.C. (2003), “Aerostatic stability analysis of suspension bridges under parametric uncertainty”, *Eng. Struct.*, **25**, 1675-1684.
- Cheng, J., Jiang, J.J., Xiao, R.C. and Xiang, H.F. (2004), “Nonlinear aerostatic stability analysis of Jiangyin suspension bridge”, *Eng. Struct.*, **24**, 773-781.
- Fu, B., Wang, Z.Y., Zhao, Y. and Yang, L. (2015), “Stochastic optimal control of stayed cable vibrations with wide-band random wind excitation using axial support motion”, *Adv. Struct. Eng.*, **18**(9), 1535-1550.
- Huang, B., Seresh, R.F. and Zhu, L.P. (2013), “Statistical analysis of basic dynamic characteristics of large span cable-stayed bridge based on high order perturbation stochastic FEM”, *Adv. Struct. Eng.*, **16**(9), 1499-1512.
- Li, Y.L., Wang, S. and Che, Y.Y. (2014a), “Analysis on aerostatic response for Hong kong-Zhuhai-Macao Great Bridge in construction stage”, *Appl. Mech. Mat.*, **455**, 220-223.
- Li, Y.L., Wang, D.X., Wu, C.P. and Chen, X.Z. (2014b), “Aerostatic and buffeting response characteristics of catwalk in a long-span suspension bridge”, *Wind Struct.*, **19**(6), 665-686.
- Ministry of Transport of the People's Republic of China. (2004), Wind-resistant Design Specification for

- Highway Bridges (JTG/T D60-01 —2004), China Communications Press, Beijing, China. (In Chinese)
- Xia, H., Roeck, G.D. and Goicolea, J.M. (2011), *Bridge Vibration and Control: New Research*, Nova Science Publishers, New York, USA.
- Xu, F.Y. and Chen, A.R. (2009), “Aerostatic response analysis on Sutong Bridge”. *Eng. Mech.*, **26** (1), 113-119 (in Chinese).
- Xu F.Y., Chen A.R., Zhang Z. (2013). “Aerostatic wind effects on the Sutong Bridge”, *Proceedings of the ISDEA 2013*, IEEE, Piscataway, USA.
- Wang, X.Y. and Xiong, R. (2011), “Study on wind resistance strategy and stability calculation of a single-span suspension bridge”, *Appl. Mech. Mat.*, **90-93**, 1082-1086.
- Zhang, W.M., Ge, Y.J. and Levitan, M.L. (2013a), “Nonlinear aerostatic stability analysis of new suspension bridges with multiple main spans”, *The Brazilian Society of Mech. Sci. Eng.*, **35**, 143-151.
- Zhang, W.M., Ge, Y.J. and Levitan, M.L. (2013b), “A method for nonlinear aerostatic stability analysis of long-span suspension bridges under yaw wind”, *Wind Struct.*, **17**(5), 553-564.
- Zhang, X.J. and Yao, M. (2015), “Numerical investigation on the wind stability of super long-span partially earth-anchored cable-stayed bridges”, *Wind Struct.*, **21**(4), 407-424.
- Zhang, J.M. (2015), “Buffeting time-domain analysis and study on wind-resistance measure under construction for super kilometer-span highway-railway steel truss cable-stayed bridge”, Master’s dissertation, *Southwest Jiaotong University*, China.

AD